Chemical Science

Accepted Manuscript

This article can be cited before page numbers have been issued, to do this please use: L. Chen, Y. Cao, H. Huo, S. Lu, Y. Hou, T. Tan, X. Li, F. Liu and M. Zhang, *Chem. Sci.*, 2025, DOI: 10.1039/D4SC07318E.

ROYAL SOCIETY OF CHEMISTRY

rsc.li/chemical-science

View Article Online
DOI: 10.1039/D4SC07318E

ARTICLE

Metallacycle-Cored Luminescent Ionic Liquid Crystals with Trigonal Symmetry

Received 00th January 20xx,
Accepted 00th January 20xx

DOI: 10.1039/x0xx00000x

Long Chen,[a,c] Yu Cao,*[a] Haohui Huo,[a] Shuai Lu,[b] Yali Hou,[a] Tianyi Tan,[a] Xiaopeng Li,[b] Feng Liu [a] and Mingming Zhang*[a]

Herein, we report the preparation of a series of metallacycle-cored liquid crystals with hexagonal and trigonal symmetry based on the self-assembly of tri(ethyl glycol) (TEG)-functionalized diplatinum(II) ligands and alkyl chain-appendant tetraphenylethene (TPE) derivatives. Interestingly, as the increase of the density of the TEG units in the metallacycles, the phase separation between TEG and alkyl chains reduces the symmetry of columnar phase from hexagonal *p6mm* to trigonal *p3m*1, which significantly enhances the aggregation of TPE units and thus increases the emission of the system, resulting in fluorescence quantum yield as high as 47.4% in mesogenic phase. Moreover, the positive charges of the metallacycles endow these liquid crystals good ionic conductivity at room temperature, making them serve as potential candidates for optoelectronics.

Introduction

Macrocycles play a vital role in the development of supramolecular chemistry for their molecular recognition and complexation properties[1-5]. Further self-assembly of macrocycles can generate favorable channels via molecular stacking, leading to the design of functional materials for the transportation of ions and molecules[6-8]. Especially, the formation of mesogenic phases will endow the materials good orientation and ordered nanostructures, making them serve as useful materials for absorption, separation, sensing and transportation[8-15]. Therefore, various covalent macrocycles have been used as the cores to prepare macrocycle-cored liquid crystals to deliver different functions[16-19]. However, this strategy generally requires tedious chemical synthesis to decorate flexible chains onto the macrocycles to benefit them enough mobility for suitable molecular stacking and liquid crystallinity[20]. In order to solve this problem, macrocycles formed by non-covalent interactions were developed,[21] with the aim to simplify the synthesis with their liquid crystalline properties well-retained.

Metal-coordination interactions have been widely applied for the construction of supramolecular coordination complexes (SCCs)[22-28] with certain stability owing to their good directionality and moderate bond strength[29-32]. These SCCs, including metallacycles and metallacages, possess well-defined shapes, sizes and geometries, making them serve as an ideal platform for the further constructing ordered supramolecular assemblies with increased complexity via hierarchical self-assembly. Therefore, various interesting supramolecular structures, including supramolecular polymers, networks and gels, liquid crystals have been prepared through SCC-based hierarchical self-assembly. Recently, we have reported a type of emissive rhomboidal metallacycle-cored liquid crystals, which exhibits columnar phase and shows the potential for the preparation of optoelectronic materials.[33] However, these liquid crystals only show moderate emission, and their conductivity has not been explored. While for liquid crystal displays (LCDs), the mesogenic materials should be both highly emissive and sufficient conductive to offer the device certain brightness, efficiency as well as electroluminescence[34-37]. Therefore, liquid crystals with high quantum yields and ion-conductivities are urgently needed for both devices and fundamental research.

Herein, we reported four hexagonal metallacycles with varied density of tri(ethylene glycol) (TEG) units (Scheme 1) which show both emission and ionic conductivity in mesogenic phase. All these metallacycles show hexagonal columnar mesophase (Col_{hex}) over a wide temperature range. In the film state, associated with the reduction of symmetry from *p6mm* to *p3m*1, the quantum yield of the metallacycle in film state reaches 47.4% at room temperature, much higher than previously reported rhomboidal metallacycle-cored liquid crystals and many other luminescent liquid crystals[33,38]. More interestingly, the ionic nanochannels formed by the stacking of these hexagonal metallacycles endow the metallacycles good ionic conductivity (1.1×10^{-6} S cm^{-1} at 30 °C) in liquid crystalline film at room temperature. This work reveals hollow hexagonal-shaped metallacycles can form stable mesophases driven by

[a] Shaanxi International Research Center for Soft Matter, State Key Laboratory for Mechanical Behavior of Materials, Xi'an Jiaotong University, Xi'an 710049, P. R. China. E-mail: yu.cao@xjtu.edu.cn; mingming.zhang@xjtu.edu.cn
[b] College of Chemistry and Environmental Engineering, Shenzhen University, Shenzhen 518055, P. R. China.
[c] Key Laboratory of Catalytic Materials and Technology of Shaanxi Province, Kaili Catalyst & New Materials Co., Ltd, Xi'an 710201, P. R. China.
Supplementary Information available: [details of any supplementary information available should be included here]. See DOI: 10.1039/x0xx00000x

View Article Online
DOI: 10.1039/D4SC07318E

metal coordination and explores a type of luminescent ionic liquid crystals that may be employed as one-dimensional ion-conductive materials in energy-related devices, optoelectronics and sensing.

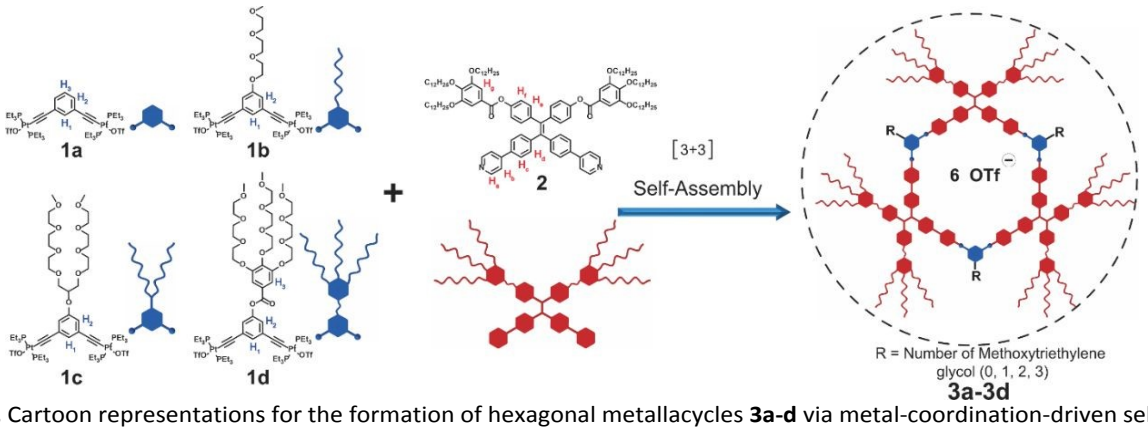

Scheme 1. Cartoon representations for the formation of hexagonal metallacycles **3a-d** via metal-coordination-driven self-assembly

Results and discussion

Based on the self-assembly of 120° platinum(II) ligands **1a-d** and a dipyridyl tetraphenylethylene (TPE) derivative **2**, hexago-nal metallacycles **3a-d** were prepared in good yields (Scheme 1). Metallacycles 3a-d were characterized by multiple NMR ($^{31}P\{^{1}H\}$, ^{1}H, and ^{13}C) analysis and electrospray ionization time-of-flight mass spectrometry (ESI-TOF-MS) (Supporting Information Figs. S1-S60). All these observations agreed well with previously reported results[33] and suggested the successful preparation of hexagonal metallacycles **3a-d**.

The liquid crystalline properties of metallacycles **3a-d** was investigated by differential scanning calorimetry (DSC), polarized optical microscopy (POM), and small/wide angle X-ray scattering (SAXS/WAXS). Taking **3d** as an example (Fig. 1a), no obvious exothermic/endothermic peaks were observed above room temperature from the DSC curves (Fig. 1b and Supporting Information Fig. S61). Clear birefringent textures were found for all the metallacycles upon heating (Fig. 1c and Supporting Information Figs. S62-S65). Due to the same phase type and close melting point between TEG chains and dodecane, the DSC curves and POM textures of **3a-d** are similar with each other. WAXS temperature scans showed an obvious diffused peaks at ca. 0.45 nm for all the metallacycles (Fig. 1d and Supporting Information Figs. S66a-d). Perticularly, an extra sharp peak at 0.37 nm was seen for **3d** until 130°C (Fig. 1d), corresponding to the π-π stacking of the adjacent metallacycles, suggesting the increased packing order as the increase of the density of TEG units. All the results suggested the formation of thermotropic liquid crystal above room temperature for all the metallacycles.

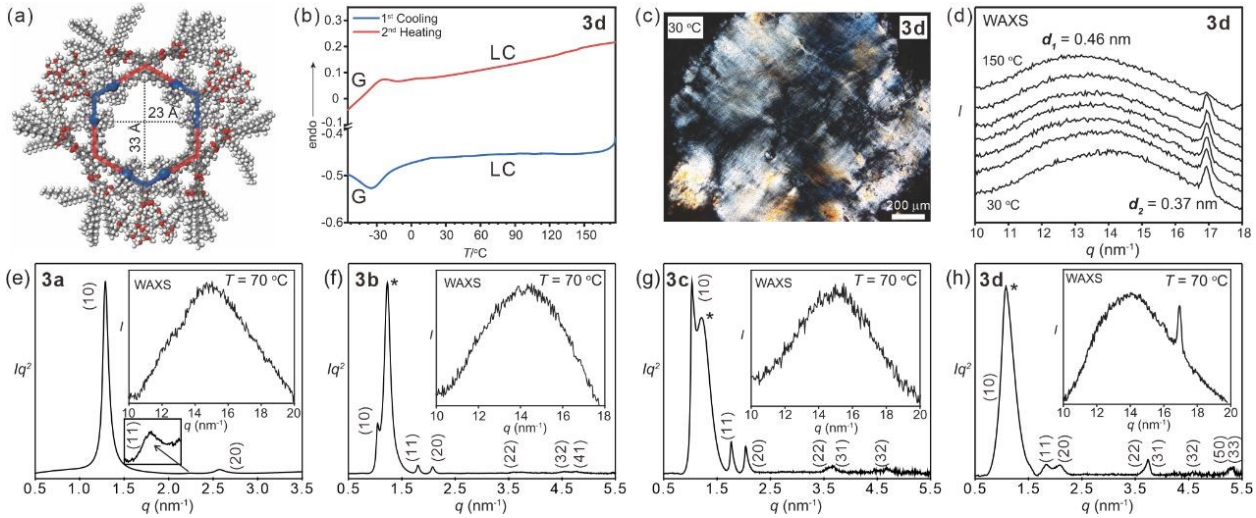

Fig 1. (a) Molecular model of **3d** optimized by molecular dynamics. The largest hole should be ca. 2.3 nm. (b) DSC curves of **3d** upon first cooling and second heating. No obvious exothermic/endothermic peaks can be observed. (c) POM texture after shearing of **3d** at room temperature, exhibiting both birefrience and fluidity. (d) WAXS temperature scan of **3d** from room temperature to 150 °C. The diffused peak d_1 and features from DSC and POM support the liquid crystalinity. Vanishing of d_2 suggests the loss of local order upon heating. (e-h) SAXS/WAXS diffractograms of metalacycles for **3a**, **3b**, **3c** and **3d** at 70 °C. The (10) peak of **3d** is labelled according to the lattice parameter determined by high index peaks.

View Article Online
DOI: 10.1039/D4SC07318E

ARTICLE

In order to decipher the liquid crystalline phase, SAXS measurements were performed for metallacycles **3a-d** (Figs. 1e-h, Supporting Information Figs. S66e-l and Supporting Information Tables S1-S4). For **3a**, the scattering pattern indicated typical hexagonal lattice with 2D symmetry as columnar phase (ratio of *d*-spacings: 1 : $1/3^{1/2}$: 1/2) (Fig. 1e). The lattice parameter a_{hex} of **3a** was 5.61 nm. The reconstructed electron density (ED) map (Fig. 2a) suggested that metallacycle **3a** self-organized into columns (Fig. 2b) owing to the steric effect and nano-segregation caused by the peripheral alkyl chains. From the hollow center (red circular region) to the metallacycles (green region) and then to the peripheral alkyl chains (purple region), the electron density increased gradually, which was consistent with the stacking of **3a** in columnar phase. Owing to the free-rotating metallacycles and adjacent holes, the spatial and temporal average ED of metallacycles was lower than peripheral alkyl chains. Interestingly, for metallacycles **3b-d**, an extra broad peak adjacent to (10) was observed (Fig. 1f-h), indicating the local clusters of TEG units, which indicates the columnar phase of *p*3*m*1 plane group (for more details, see Section S7 and Fig. S67).[33] Correspondingly, the lattice parameter of metallacycles **3b-d** swelled to ca. 6.96 nm. The phase separation would inevitably induce the symmetry breaking and reduction of symmetry from hexagonal *p6mm* for **3a** to trigonal *p*3*m*1 for **3b-d**. The rarely found *p*3*m*1 phase was only observed in the bent-core bola-polyphile liquid crystal due to steric effect.[39] Due to its non-centrosymmetric property, the phase combination becomes arbitrary which hinders the reconstruction of ED map by simple trial and error. Thus, a theoretical packing model with actual lattice parameter, molecular size and electron density was constructed to estimate the phase angle combination (Fig. 2c and Supporting Information Section 7). The Fourier transform of the model, based on positions and shape factor of circular and rectangular components in the proposed model, gives analytical scattering Intensities fit well with experimental results with phase angle combination (Fig. 2d and Supporting Information Table S5). An alternating ED distribution was seen at the corners of metallacycles **3b-d** based on both experimental and simulated results (Fig. 2e-f and Supporting Information Fig. S68), suggesting the rotation of the metallacycles was restricted by the aggregation of peripheral TEG and alkyl chains (Fig. 2g), which would benefit for the emission of these metallacycles.

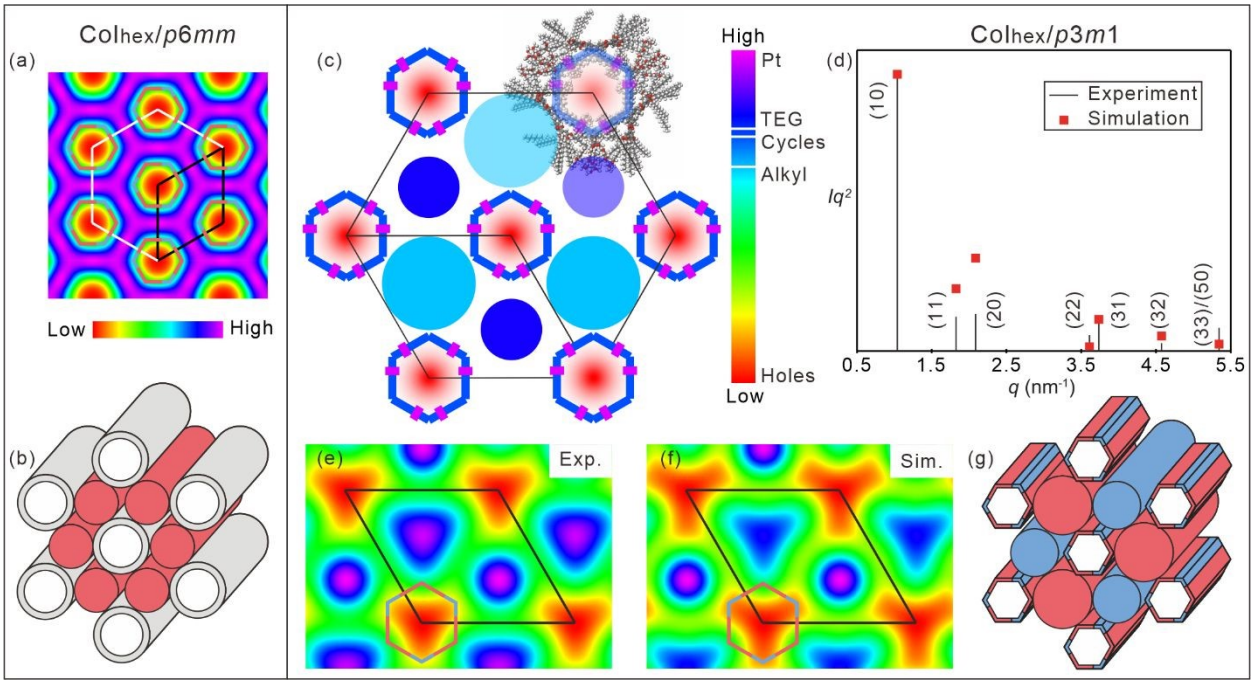

Fig 2. (a) Reconstructed electron density maps and (b) schematic model of Col_{hex}/*p6mm* phase. The metallacycles free rotate to generate the uniform ED in green. (c) Model constructed for Col_{hex}/*p*3*m*1 phase whose colors are from the normalized electron density. (d) The experimental and simulated SAXS intensities of the indexed peaks. (e, f) Reconstructed electron density maps based on experimental intensities and simulated intensities. The main deviation is from the ED of alkyl chains. (g) Schematic model of Col_{hex}/*p*3*m*1 phase.

The UV-vis absorption and emission spectra of metallacycles **3a-d** in dichloromethane were collected (Fig. 3a and Supporting Information Fig. S69a-h). All these metallacycles exhibited three absorption bands centered at ca. 266 nm, 299 nm and 357 nm

and a broad emission band centered at 510 nm, which was attributed to the characteristic of TPE units.[33] Upon the gradual addition of hexane into the dichloromethane solution of metallacycles **3a-d**, their emission increased remarkably (Fig. 3b and Supporting Information Fig. S69i-l), suggesting that the aggregation-induced emission (AIE)[40] feature of TPE was well retained. Thin films of metallacycles **3a-d** were further prepared to study their absorption and emission in the liquid crystalline state at room temperature (Fig. 3c). Three absorption bands centered at 276 nm, 304 and 339 nm were found owing to n–σ*, n–π* and π–π* transitions, respectively. These metallacycles exhibited a single emission band with maximum emission centered at 493 nm. The quantum yields (Φ_F) were measured to be 22.8% for **3a**, 18.0% for **3b**, 24.9% for **3c**, and 47.4% for **3d** (Fig. 3d), which were among the highest values of luminescent liquid crystal at room temperature (Fig. S70a).[38]

Apart from the luminescence from aggregation, the columnar phase provided intrinsic 1D channels (Fig. 3e). Combining with the positive-charged nature of these metallacycles and the ionic conductivity of TEG units,[41] the ionic conductivities of **3a-d** along the columnar axis were measured by electrochemical impedance spectroscopy. As shown in Fig. 3f, the ionic conductivities of metallacycles **3a-d** increased along with temperature due to the enhanced mobility. At 30 °C, the ionic conductivity was 5.5×10^{-7} S cm^{-1} for **3a**, 6.9×10^{-7} S cm^{-1} for **3b**, 9.4×10^{-7} S cm^{-1} for **3c** and 1.1×10^{-6} S cm^{-1} for **3d**. As the increase of the density of TEG units, the ionic mobility of the metallacycles in the mesophase was enhanced, giving better ionic conductivity comparable with other ionic liquid crystals at room temperature (Fig. S70b).[42] Integrating with their highly emissive nature and ease of alignment, these metallacycles could be applied in the construction of optoelectrical devices such as LCDs.

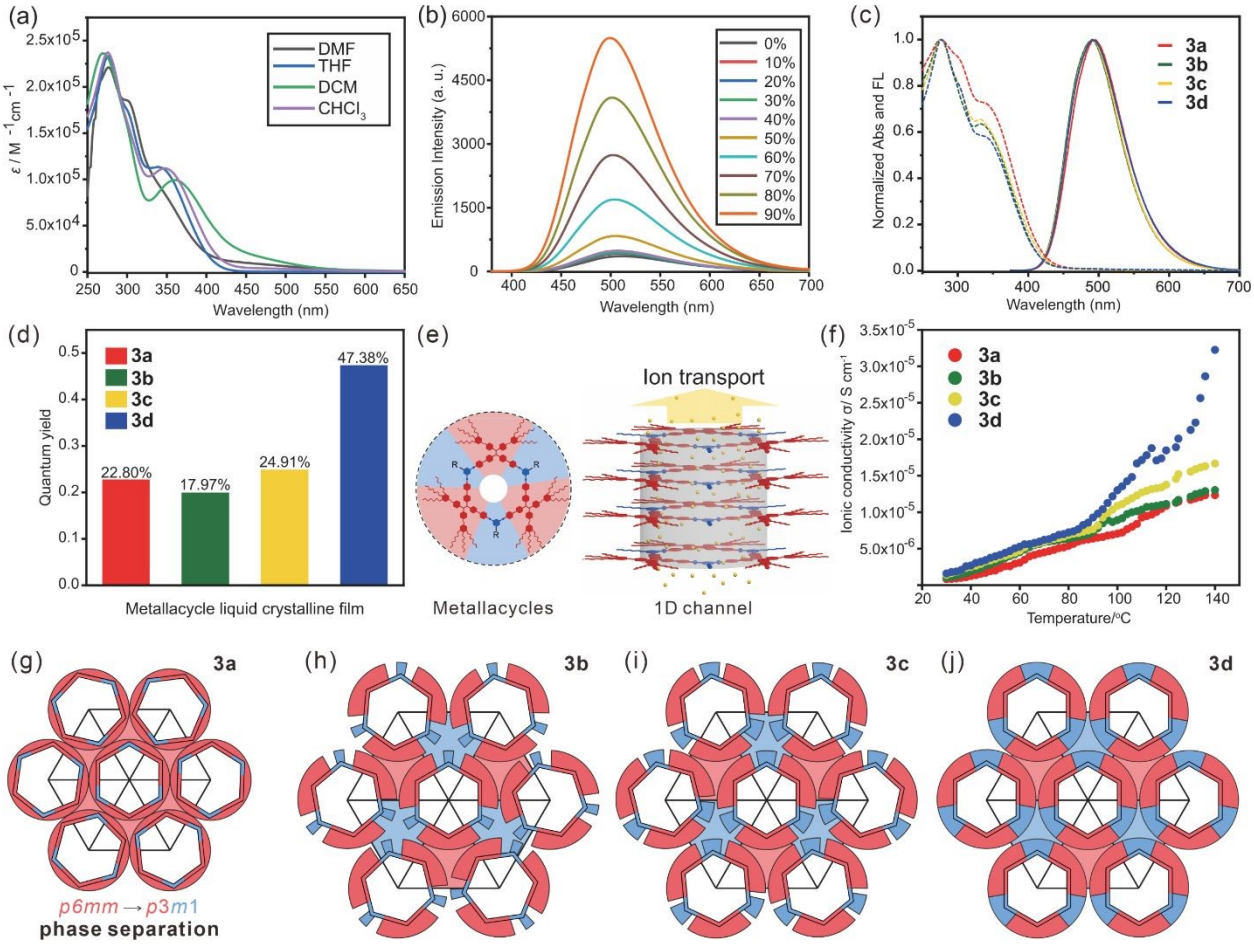

Fig 3. (a) UV/vis absorption spectra of metallacycyes **3d** in different solvents. (b) Emission spectra of **3d** in dichloromethane/hexane (λ_{ex} = 365 nm, c = 10 μM), suggesting the AIE property. (c) Absorption (dashed line), fluorescence emission spectra (solid line) of the liquid crystal film of metallacycles **3a**-**d**. (d) quantum yield (Φ_F) of liquid crystal film of metallacycles **3a**-**d**. (e) Schematic illustration of the metallacycles and their aggregation with 1D channel. (f) Ionic conductivities as a function of temperature of metallacycles **3a**-**d** in the aligned columnar phases. (g-j) Schematic illustration of the packing of metallacycles **3a-d** in the columnar phases. Introduction of TEG units reduces hexagonal *p*6*mm* group (6-fold red shadow) into trigonal *p*3*m*1 group (3-fold red/blue shadow).

Both liquid crystalline phase and properties of these metallacycles were closely related with the phase separation and symmetry breaking. As indicated by ED maps (Fig. 2a, e), metallacycles **3a-d** were packed in columnar phase with central hollow of ca. 2.1 nm, close to their geometrically optimized molecular model (Fig. 1a). Such similarity suggested minor local

shift in crystallographic plane, generating well-organized channels along columnar axis capable of transporting ions. In order to evaluate the influence of in-plane steric effect, molecular packing models based on actual molecular shape and peripheral chains distribution were proposed (Fig. 3g-j). Alkyl chains in red uniformly filled the space between columns of **3a**, providing liquid crystallinity and conventional *p6mm* group.[43] Alkyl chains of **3b-d** were rearranged with blue TPE units as interval due to phase separation, forming *p*3*m*1 phase. Obviously, the volume of TPE units was essential for the metallacycle packing. Theoretically, 54.1% volume ratio between TEG and alkyl chains (Supporting information Fig. S71) was needed to properly fill the space between neighboring columns. The volume ratio was 11.9% for **3b**, leading to inevitable local rotation and lowest Φ_F as 17.8%. Increasing of the volume of TEG units gradually restricted the rotation of the metallacycles and thus enhanced the emission of metallacycles **3b-d**. **3d** provided a more desirable volume ratio as large as 42.6%, giving a strong phase separation and good space filling to regulate the stacking of metallacycles and eventually boost the Φ_F to 47.4%.

Conclusions

In summary, we have successfully constructed a series of hexagonal metallacycles that formed thermotropic hexagonal columnar mesophase at room temperature. The phase separation inside these liquid crystals further restricts the molecular motion of these metallacycles, benefiting them with good emission in the film state. Moreover, the ordered packing of these metallacycles in mesophase offers an organized one-dimensional channel, giving them good ionic conductivity. This study provides a simple yet effective strategy for the construction of highly emissive and ionic conductive liquid crystals via metal-coordination-driven self-assembly, which will open a new avenue for advanced supramolecular materials towards optoelectrical applications.[44-45]

Experimental methods

All reagents and deuterated solvents purchased as analytical grade and used without further purification. Column chromatography was performed using 300-400 mesh silica gel. Nuclear magnetic resonance spectra were afforded with Bruker Avance 400 MHz or 600 MHz pectrometer. ^{1}H and ^{13}C NMR chemical shifts are reported relative to residual solvent signals, and $^{31}P\{^{1}H\}$ NMR chemical shifts are referenced to an external unlocked sample of 85% H_3PO_4 (δ 0.0). Mass spectra were recorded on a Micromass Quattro II triple-quadrupole mass spectrometer using electrospray ionization with a MassLynx operating system. The UV-vis experiments were conducted on Lambd 950 absorption spectrophotometer. The fluorescent experiments were conducted on a Hitachi F-7000 fluorescence spectrophotometer. Phase textures of all compounds were fully characterized by polarizing optical microscopy (Olympus BX51-P) in conjunction with a heating stage (Linkam LTS420E) and controller (T95-HS). Optical investigations were carried out under equilibrium conditions between two glass slides that were used without further treatment. Transition enthalpies were determined as obtained from differential scanning calorimetry (DSC) which were recorded on a TA DSC250 (heating and cooling rate: 10 K/min, peak temperatures). SAXS were conducted in BL16B1 of SSRF and processed by Nika and Irena macros from Igor platform.

Author contributions

L. C.: Data Curation, Investigation, Validation, Writing – Original Draft. Y. C.: Formal Analysis, Funding Acquisition, Investigation, Methodology, Visualization, Writing – Review & Editing. H. H.: Investigation, Writing – Review & Editing. S. L.: Investigation, Writing – Review & Editing. Y. H.: Investigation, Writing – Review & Editing. T. T.: Investigation, Writing – Review & Editing. X. L.: Project Administration, Writing – Review & Editing. F. L.: Project Administration, Supervision, Writing – Review & Editing. M. Z.: Conceptualization, Funding Acquisition, Project Administration, Resources, Supervision, Writing – Review & Editing.

Conflicts of interest

There are no conflicts to declare.

Data availability

The data supporting this study are available in the ESI of this article.

Acknowledgements

This work was supported by the National Natural Science Foundation of China (22171219, 22222112 and 12204369), China Postdoctoral Science Foundation (2022M712551, 2023T160505), Innovation Talent Promotion Plan of Shaanxi Province for Science and Technology Innovation Team (2023-CX-TD-51), and Science and Technology Agency of Shaanxi Province (2023-YBGY-459, 2024JC-YBQN-0116). The authors thank beamlines BL16B1 at Shanghai Synchrotron Radiation Facility (SSRF) for providing the beam time. We also thank Dr. Gang Chang and Dan He at Instrument Analysis Center at Instrument Analysis Center of Xi'an Jiaotong University for NMR and fluorescence measurements.

References

1 Z. Liu, S. K. M. Nalluri, J. F. Stoddart, *Chem. Soc. Rev.* 2017, ***46***, 2459-2478.
2 D. Prochowicz, A. Kornowicz, J. Lewiński, *Chem. Rev.* 2017, ***117***, 13461-13501.
3 R. Kumar, A. Sharma, H. Singh, P. Suating, H. S. Kim, K. Sunwoo, I. Shim, B. C. Gibb, J. S. Kim, *Chem. Rev.* 2019, ***119***, 9657-9721.
4 S. J. Barrow, S. Kasera, M. J. Rowland, J. Del Barrio, O. A. Scherman, *Chem. Rev.* 2015, ***115***, 12320-12406.

DOI: 10.1039/D4SC07318E

5 T. Ogoshi, T. Yamagishi, Y. Nakamoto, *Chem. Rev.* 2016, ***116***, 7937-8002.
6 Q. Wang, Y. Zhong, D. P. Miller, X. Lu, Q. Tang, Z. L. Lu, E. Zurek, R. Liu, B. Gong, *J. Am. Chem. Soc.* 2020, ***142***, 2915-2924.
7 M. Stepien, B. Donnio, J. L. Sessler, *Angew. Chem. Int. Ed.* 2007, ***46***, 1431-1435.
8 Y. Luo, N. Marets, T. Kato, *Chem. Sci.* 2018, ***9***, 608-616.
9 M. Fritzsche, A. Bohle, D. Dudenko, U. Baumeister, D. Sebastiani, G. Richardt, H. W. Spiess, M. R. Hansen, S. Hoger, *Angew. Chem. Int. Ed.* 2011, ***50***, 3030-3089.
10 M. Amorin, A. Perez, J. Barbera, H. L. Ozores, J. L. Serrano, J. R. Granja, T. Sierra, *Chem. Commun.* 2014, ***50***, 688-690.
11 K. Guy, P. Ehni, S. Paofai, R. Forschner, C. Roiland, M. Amela-Cortes, S. Cordier, S. Laschat, Y. Molard, *Angew. Chem. Int. Ed.* 2018, ***57***, 11692-11696.
12 P. L. Champagne, D. Ester, D. Polan, V. E. Williams, V. Thangadurai, C. C. Ling, *J. Am. Chem. Soc.* 2019, ***141***, 9217-9224.
13 Y. X. Hu, X. Hao, L. Xu, X. Xie, B. Xiong, Z. Hu, H. Sun, G. Q. Yin, X. Li, H. Peng, H. B. Yang, *J. Am. Chem. Soc.* 2020, ***142***, 6285-6294.
14 Y. X. Hu, X. Hao, D. Wang, Z. C. Zhang, H. Sun, X. D. Xu, X. Xie, X. Shi, H. Peng, H. B. Yang, X. Lin, *Angew. Chem. Int. Ed.* 2024, ***63***, e202315061.
15 T. Kato, J. Uchida, T. Ichikawa, T. Sakamoto, *Angew. Chem. Int. Ed.* 2018, ***57***, 4355-4371.
16 Z. Yu, X. M. Chen, Z. Y. Liu, M. Wang, S. Huang, H. Yang, *Chem. Commun.* 2021, ***57***, 911-914.
17 K. Sato, Y. Itoh, T. Aida, *J. Am. Chem. Soc.* 2011, ***133***, 13767-13769.
18 S. Kawano, Y. Ishida, K. Tanaka, *J. Am. Chem. Soc.* 2015, ***137***, 2295-2302.
19 Y. Li, H. Su, X. Feng, K. Yue, Z. Wang, Z. Lin, X. Zhu, Q. Fu, Z. Zhang, S. Z. D. Cheng, W. B. Zhang, *Polym. Chem.* 2015, ***6***, 827-837.
20 W. Zhang, J. S. Moore, *Angew. Chem. Int. Ed.* 2006, ***45***, 4416-4439.
21 H. Y. Lin, Y. T. Wang, X. Shi, H. B. Yang, L. Xu, *Chem. Soc. Rev.* 2023, ***52***, 1129-1154.
22 Z. Zhang, Z. Zhao, Y. Hou, H. Wang, X. Li, G. He, M. Zhang, *Angew. Chem. Int. Ed.* 2019, ***58***, 8862-8866.
23 Z. Zhang, Z. Zhao, L. Wu, S. Lu, S. Ling, G. Li, L. Xu, L. Ma, Y. Hou, X. Wang, X. Li, G. He, K. Wang, B. Zou, M. Zhang, *J. Am. Chem. Soc.* 2020, ***142***, 2592-2600.
24 Y. Hou, Z. Zhang, S. Lu, J. Yuan, Q. Zhu, W. P. Chen, S. Ling, X. Li, Y.-Z. Zheng, K. Zhu, M. Zhang, *J. Am. Chem. Soc.* 2020, ***142***, 18763-18768.
25 C. Mu, Z. Zhang, Y. Hou, H. Liu, L. Ma, X. Li, S. Ling, G. He, M. Zhang, *Angew. Chem. Int. Ed.* 2021, ***133***, 12401-12405.
26 Y. Hou, Z. Zhang, L. Ma, R. Shi, S. Ling, X. Li, G. He, M. Zhang, *CCS Chem.* 2022, ***4***, 2604-2611.
27 C. Mu, L. Zhang, G. Li, Y. Hou, H. Liu, Z. Zhang, R. Zhang, T. Gao, Y. Qian, C. Guo, G. He, M. Zhang, *Angew. Chem. Int. Ed.* 2023, ***135***, e202311137.
28 K. Gao, Y. Cheng, Z. Zhang, X. Huo, C. Guo, W. Fu, J. Xu, G. L.; Hou, X. Shang, M. Zhang, *Angew. Chem. Int. Ed.* 2024, ***136***, e202319488.
29 B. H. Northrop, Y. R. Zheng, C. Ki-Whan, P. J. Stang, *Acc. Chem. Res.* 2009, ***42***, 1554-1563.
30 T. R. Cook, Y.-R. Zheng, P. J. Stang, *Chem. Rev.* 2013, ***113***, 734-777.
31 T. R. Cook, P. J. Stang, *Chem. Rev.* 2015, ***115***, 7001-7045.
32 Z. L. Gong, Z. Q. Li, Y. W. Zhong, *Aggregate* 2022, ***3***, e177.
33 L. Chen, C. Chen, Y. Sun, S. Lu, H. Huo, T. Tan, A. Li, X. Li, G. Ungar, F. Liu, M. Zhang, *Angew. Chem. Int. Ed.* 2020, ***132***, 10143-10150.
34 Y. F. Wang, J. W. Shi, J. H. Chen, W. G. Zhu, E. Baranoff, *J. Mater. Chem. C* 2015, ***3***, 7993-8005.
35 D. Zhao, H. He, X. Gu, L. Guo, K. S. Wong, J. W. Y. Lam, B. Z. Tang, *Adv. Opt. Mater.* 2016, ***4***, 534-539.
36 J. Han, S. Guo, H. Lu, S. Liu, Q. Zhao, W. Huang, *Adv. Opt. Mater.* 2018, ***6***, 1800538.
37 Y. Wu, L. H. You, Z.-Q. Yu, J.-H. Wang, Z. Meng, Y. Liu, X.-S. Li, K. Fu, X.-K. Ren, B. Z. Tang, *ACS Mater. Lett.* 2020, ***2***, 505-510.
38 C. Cuerva, M. Cane, C. Lodeiro, *Chem. Rev.* 2021, ***121***, 12107-13010.
39 B. Glettner, F. Liu, X. B. Zeng, M. Prehm, U. Baumeister, G. Ungar, C. Tschierske, *Angew. Chem. Int. Ed.* 2008, ***47***, 6080-6083.
40 J. Mei, N. L. C. Leung, R. T. K. Kwok, J. W. Y. Lam, B. Z. Tang, *Chem. Rev.* 2015, ***115***, 11718-11940.
41 Z. Su, J. Huang, W. Shan, X. Y. Yan, R. Zhang, T. Liu, Y. Liu, Q. Y. Guo, F. Bian, X. Miao, M. Huang, S. Z. D. Cheng, *CCS Chem*. 2021, ***3***, 1434-1444.
42 S. Dou, S. Zhang, R. J. Klein, J. Runt, R. H. Colby, *Chem. Mater.* 2006, ***18***, 4288-4295.
43 K. Goossens, K. Lava, C. R. Bielawski, K. Binnemans, *Chem. Rev.* 2016, ***116***, 4643-4807.
44 B. Soberats, M. Yoshio, T. Ichikawa, H. Ohno, T. Kato, *J. Mater. Chem. A.* 2015, ***3***, 11232-11238.
45 B. Soberats, M. Yoshio, T. Ichikawa, X. B. Zeng, H. Ohno, G. Ungar, T. Kato, *J. Am. Chem. Soc.* 2015, ***137***, 13212-13215.

View Article Online
DOI: 10.1039/D4SC07318E

The data supporting this article have been included as part of the Supplementary Information.